

# Apolipoprotein M attenuates age-related macular degeneration phenotypes via sphingosine-1-phosphate signaling and lysosomal lipid catabolism

Received: 20 June 2024

Accepted: 3 June 2025

Published online: 24 June 2025

 Check for updates

Tae Jun Lee<sup>1,2</sup>, Andrea Santeford<sup>1</sup>, Kristen M. Pitts<sup>1</sup>, Carla Valenzuela Ripoll<sup>3</sup>, Ryo Terao<sup>1,4</sup>, Zhen Guo<sup>3</sup>, Mualla Ozcan<sup>3</sup>, Dagmar Kratky<sup>5,6</sup>, Christina Christoffersen<sup>7,8</sup>, Ali Javaheri<sup>3,9</sup> ✉ & Rajendra S. Apte<sup>1,2</sup> ✉

Age-related macular degeneration (AMD) is a leading cause of blindness in people over 50. AMD and cardiovascular disease share risk factors including age, impaired lipid metabolism, and extracellular lipid deposition. Because of its importance in age-related diseases, we hypothesize that apolipoprotein M (ApoM), a lipocalin that binds sphingosine-1-phosphate (S1P), might restore lipid homeostasis and retinal function in AMD. In support, we find that human patients with AMD demonstrate significantly reduced ApoM compared to controls. In mice with impaired retinal cholesterol efflux, ApoM improves retinal pigment epithelium (RPE) function and lipotoxicity in an S1P- and S1P receptor 3-dependent manner. Ultrastructural evidence of enhanced melanosome-lipid droplet interactions led us to hypothesize and demonstrate that ApoM-S1P signaling drives RPE-specific lysosomal lipid catabolism. RPE-specific knockout of lysosomal acid lipase recapitulates features of AMD. Our study defines a novel role for ApoM/S1P signaling in AMD driven by RPE lipotoxicity, mediated by cell-autonomous lysosomal lipid catabolism.

Age-related macular degeneration (AMD) is the leading cause of blindness among Americans over 50<sup>1–3</sup>. In its early and intermediate stages, AMD is marked by the buildup of lipoprotein-rich deposits—either under the neurosensory retina (sub-retinal drusenoid deposits, or SDD) or beneath the retinal pigment epithelium (RPE), known as drusen<sup>4,5</sup>. Vision loss occurs when AMD advances to one of its two late-stage forms. The first, known as “wet” AMD, involves abnormal blood vessel growth (choroidal neovascularization or CNV). Though it represents only about 20% of advanced cases, it accounts for roughly

80% of AMD-related vision loss<sup>6</sup>. The second form, advanced “dry” AMD, progresses to geographic atrophy (GA), a condition characterized by the atrophic degeneration of retinal neurons<sup>7</sup>.

Current treatments are limited to the advanced stages of the disease<sup>8</sup>. The only recommended intervention for early or intermediate AMD is micronutrient supplementation<sup>1,9</sup>. This underscores a critical gap in our understanding of the molecular mechanisms driving early dry AMD, and the lack of effective strategies to prevent its progression to GA or CNV and resulting vision loss. Anti-VEGF injections

<sup>1</sup>John F. Hardesty, MD Department of Ophthalmology and Visual Sciences, Washington University in St. Louis School of Medicine, St. Louis, MO, USA.

<sup>2</sup>Department of Developmental Biology, Washington University in St. Louis School of Medicine, St. Louis, MO, USA. <sup>3</sup>Department of Medicine, Washington University in St. Louis School of Medicine, St. Louis, MO, USA. <sup>4</sup>Department of Ophthalmology, Graduate School of Medicine, University of Tokyo, Tokyo, Japan. <sup>5</sup>Gottfried Schatz Research Center, Molecular Biology and Biochemistry, Medical University of Graz, Graz, Austria. <sup>6</sup>BioTechMed-Graz, Graz, Austria. <sup>7</sup>Department of Biomedical Sciences, University of Copenhagen, Copenhagen, Denmark. <sup>8</sup>Department of Clinical Biochemistry, Rigshospitalet, University of Copenhagen, Copenhagen, Denmark. <sup>9</sup>John Cochran VA Hospital, St Louis, MO, USA. ✉e-mail: [ali.javaheri@wustl.edu](mailto:ali.javaheri@wustl.edu); [apte@wustl.edu](mailto:apte@wustl.edu)

are used to manage wet AMD by reducing the risk of sudden vision loss, but they do not halt the ongoing neurodegeneration associated with the underlying dry form<sup>10–12</sup>. For GA, recently approved intravitreal C3 and C5 complement inhibitors offer only modest slowing of disease progression and carry risks such as conversion to wet AMD and retinal vasculitis<sup>13,14</sup>. These limitations highlight the need for novel and aggressive approaches to prevent the progression of AMD to its vision-compromising stages.

Currently, there are no curative treatments for early or intermediate dry AMD at any stage. Recent studies, including work from our laboratory, have highlighted the pivotal role of cholesterol and lipid accumulation in the initiation and progression of AMD<sup>4,7,15</sup>. Despite growing recognition that lipid buildup is a key driver of disease progression and vision loss, no therapeutic strategies have been developed to target this underlying cause of AMD. This critical gap underscores the urgent need for innovative approaches that directly address lipid accumulation as a therapeutic target.

In AMD, lipoprotein accumulation and thickening of Bruch's membrane—the basement membrane beneath retinal pigment epithelial (RPE) cells—disrupt essential solute and lipid transport<sup>5,16–18</sup>. Lipid homeostasis in the RPE is typically regulated by the body's reverse cholesterol transport (RCT) system, primarily through high-density lipoprotein (HDL) particles<sup>19</sup>. A key protein in HDL, apolipoprotein A-I (ApoA-I) plays a critical role in RCT by facilitating the removal of cholesterol from extrahepatic tissues. However, impaired RCT leads to the buildup of lipoproteins beneath the retina and RPE, contributing to the hallmark features of AMD<sup>4,5</sup>. Genetic studies have linked polymorphisms in lipid pathway genes—particularly those involved in cholesterol efflux, the initial step in RCT—to increased AMD risk<sup>20–22</sup>. Furthermore, clinical cohort studies have revealed serum dyslipidemia in AMD patients, supporting the role of lipid imbalance in disease progression<sup>4,15,23,24</sup>. These findings suggest that promoting the removal of cholesterol and lipids from the sub-retinal space, RPE, and Bruch's membrane could prevent or slow the formation of drusenoid deposits during the early and intermediate stages of AMD<sup>25</sup>. Supporting this notion, murine models with knockouts of key genes in cholesterol metabolism, such as ATP binding cassette subfamily A member 1 (*Abca1*) and ATP binding cassette subfamily G member 1 (*Abcg1*), in rod photoreceptors, RPE, and myeloid cells exhibit dry AMD-like phenotypes<sup>26–29</sup>. Human genetic evidence and murine model data underscore the importance of cholesterol metabolism in RPE survival and function. Therefore, strategies to enhance RPE lipid catabolism may offer promising therapeutic avenues to mitigate AMD progression.

Based on its involvement in aging-related disease and cholesterol metabolism, we hypothesized that the lipocalin apolipoprotein M (ApoM) may play an important role in AMD<sup>30,31</sup>. Apolipoprotein M (ApoM) is primarily produced by the liver, with a smaller contribution from the kidneys. It binds directly to sphingosine-1-phosphate (SIP)<sup>32</sup>, a bioactive sphingosine that activates SIP receptors found on various cell types, including RPE cells. Although ApoM makes up only about 5% of HDL and less than 2% of low-density lipoprotein (LDL) particles, it is responsible for binding approximately 70% of circulating SIP<sup>33–35</sup>. ApoM has a broad range of pleiotropic effects, including antioxidant and anti-atherogenic properties<sup>36,37</sup>, modulation of inflammation, endothelial protection<sup>32,38</sup>, and promotion of cell survival<sup>39</sup>. In mice with hepatocyte-specific overexpression of human APOM (ApoM<sup>TG</sup>), plasma ApoM levels increase 3–5 fold, leading to elevated plasma SIP levels<sup>35</sup>. Conversely, ApoM knockout mice (ApoM<sup>KO</sup>) show a 50% reduction in plasma SIP, with no detectable SIP on HDL but normal levels on albumin<sup>32</sup>. Additionally, ApoM has also been identified as a regulator of lysosomal function in the murine heart<sup>40</sup>.

Despite evidence linking ApoM to aging, RCT, and lysosomes, few investigations have explored the role of ApoM in AMD<sup>41,42</sup>. With

knowledge of ApoM connected to cholesterol efflux and SIP receptor signaling<sup>43</sup>, we hypothesized that ApoM and SIP receptor signaling could be involved in AMD pathogenesis. We also considered melanosomes within the RPE could play a role in ApoM-related AMD progression as they are involved in the biogenesis of lysosomal-related organelles and aiding phagosomes by fusion in stressed conditions<sup>44–46</sup>. In plasma samples from individuals with AMD, we observed significantly reduced levels of ApoM compared to healthy controls. When plasma from ApoM overexpressing mice was administered to mice with *Abca1* and *Abcg1* double knockouts in rod photoreceptors (*Abca1/g1<sup>rod/rod</sup>*), the development of AMD-like phenotypes was attenuated. In contrast, plasma from ApoM knockout mice had no such effect. Electron microscopy of the retinas from these mice revealed that ApoM appeared to enhance lysosomal lipid catabolism, as evidenced by a decrease in the overall number of lipid droplets, with more lipid droplets found interacting with melanosomes. The deletion of SIP receptor 3 (SIPR3) resulted in an AMD-like phenotype, with electron microscopy showing impaired lipid homeostasis and an increase in lipid droplets within the RPE. Similarly, both whole-body and RPE-specific knockout of lysosomal acid lipase (LAL, gene name *Lipa*), an enzyme essential for lysosomal cholesterol and triglyceride breakdown, reproduced the dry AMD-like phenotype seen in *Abca1/Abcg1<sup>rod/rod</sup>* mice. ApoM rich plasma did not rescue either SIPR3 knockout or RPE-specific LAL knockouts, suggesting that ApoM regulates SIP signaling to mediate lipid breakdown in the RPE and help prevent the development of dry AMD phenotypes.

## Results

### Patients with AMD have lower levels of circulating ApoM

To investigate a correlation between circulating ApoM and AMD, we measured plasma ApoM in age-matched patients with and without AMD by ELISA, the gold standard for measuring ApoM<sup>47,48</sup>. We measured plasma ApoM in patients diagnosed with AMD ( $n = 53$ ) and compared their levels to age-matched controls without AMD ( $n = 328$ ) (Fig. 1A). Patients with AMD had significantly decreased levels of ApoM compared to patients without AMD. These data support a potential role for circulating ApoM in AMD pathogenesis.

### ApoM ameliorates RPE functional deficits in a murine dry AMD-like model

A prior investigation from our laboratory established a dry AMD-like model by conditionally knocking out the cholesterol efflux transporters, *Abca1* and *Abcg1*, in rod photoreceptors in mice (*Abca1/g1<sup>rod/rod</sup>*). After high fat diet treatment (60% kcal from fat, 25% kcal from carbohydrate, and 15% kcal from protein) for six weeks, *Abca1/g1<sup>rod/rod</sup>* demonstrated an accelerated neurodegenerative phenotype associated with excessive accumulation of lipid in the RPE<sup>26</sup>. We also considered utilizing the mouse model of conditional RPE knockout of *Abca1* and *Abcg1*<sup>27</sup>, but the accelerated neurodegeneration seen in this model did not offer a potential opportunity for early intervention in examining the role of ApoM.

We sought to test if concurrent plasma transfer from ApoM transgenic mice that overproduce ApoM (ApoM<sup>TG</sup>) could ameliorate the RPE and photoreceptor phenotype seen in high fat diet fed *Abca1/g1<sup>rod/rod</sup>* mice. Plasma transfer of ApoM<sup>TG</sup> mice has been validated as a strategy for ApoM delivery<sup>40</sup>. We utilized plasma from ApoM knockout mice (ApoM<sup>KO</sup>) as controls. High fat diet fed *Abca1/g1<sup>rod/rod</sup>* mice were injected with 120  $\mu$ L of either ApoM<sup>TG</sup> or ApoM<sup>KO</sup> plasma every other day (Fig. 1B). Using the light bleach dark adaptation electroretinography technique<sup>28</sup>, we measured RPE function and found significant improvements in the ApoM<sup>TG</sup> plasma-treated mice by scotopic a-wave maximum measurements (Fig. 1C). These findings suggest that the RPE of ApoM<sup>TG</sup> plasma-treated *Abca1/g1<sup>rod/rod</sup>* mice functionally improved.

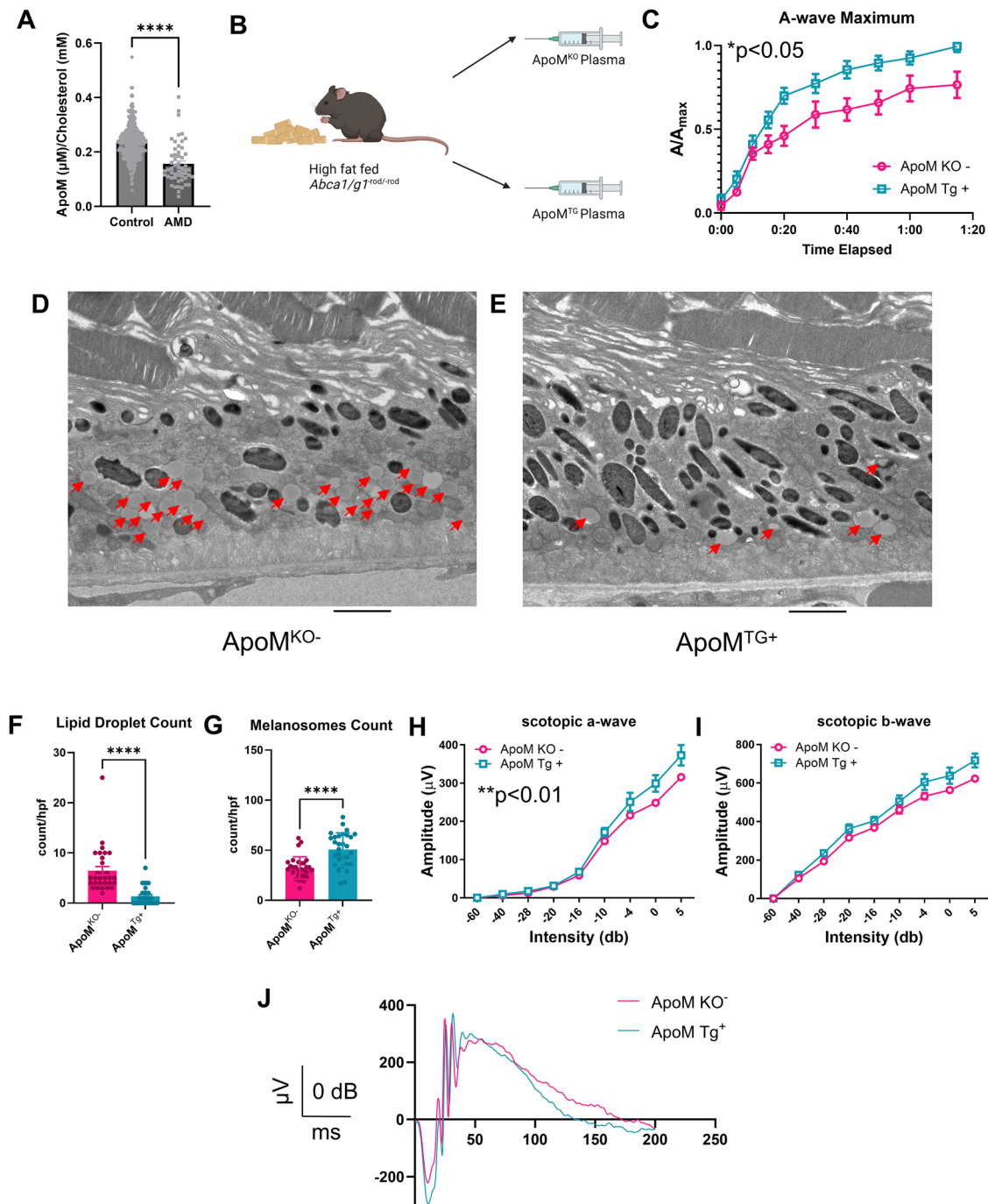


**Fig. 1 | ApoM therapy ameliorates a dry AMD-like phenotype.** **A** ApoM levels controlled to total cholesterol levels were measured in patients with ( $n = 53$ ) or without AMD ( $n = 328$ ) aged 65 and over. Patients with AMD had significantly lower ApoM levels compared to those without AMD ( $****p = 0.0000000006$ , two-tailed Welch's  $t$ -test). **B** High fat diet fed *Abca1/g1<sup>rod/rod</sup>* mice were treated with either ApoM<sup>KO</sup> or ApoM<sup>TG</sup> plasma (created in BioRender. Lee, T. (2025) <https://BioRender.com/li4w1zf>). **C** RPE functional assessment using light bleach dark adaptation electroretinography ( $n = 6$ ) revealed significantly improved functional recovery in ApoM<sup>TG</sup> plasma treated mice ( $*p = 0.0271$ , Two-way ANOVA). **D, E** Representative TEM imaging of RPE from either ApoM<sup>KO</sup> or ApoM<sup>TG</sup> plasma treated *Abca1/g1<sup>rod/rod</sup>* mice. Red arrows point to lipid droplets. **F** Quantitative assessment of lipid droplets

per high-powered field within the RPE ( $n = 30$ ) revealed significantly reduced lipid droplets in ApoM<sup>TG</sup> plasma treated mice ( $****p = 0.0000011$ , two-tailed Welch's  $t$ -test). **G** Quantitative assessment of melanosomes per high-powered field within the RPE ( $n = 30$ ) revealed significantly increased melanosome counts in ApoM<sup>TG</sup> plasma treated mice ( $***p = 0.0000068$ , two-tailed Welch's  $t$ -test). Full-field scotopic electroretinography ( $n = 6$ ) demonstrated improved **H** rod photoreceptor ( $*p = 0.0343$ , Two-way ANOVA) but not **I** inner retina (Two-way ANOVA) function in ApoM<sup>TG</sup> plasma-treated mice. **J** Representative traces of 0 dB intensity flashes show an improved waveform from ApoM<sup>TG</sup> injected mice. The scale bar represents 2  $\mu\text{m}$ . Values are mean  $\pm$  SE. Source data are provided as a Source Data file.

### RPE lipid accumulation is significantly reduced by ApoM plasma transfer

We next assessed the ultrastructural effects of ApoM treatment paradigm in the high fat diet fed *Abca1/g1<sup>rod/rod</sup>* model using electron

microscopy. These mice have previously been shown to have increased lipid droplets in the RPE<sup>26</sup>. We discovered that ApoM<sup>TG</sup> plasma-treated *Abca1/g1<sup>rod/rod</sup>* mice had significantly fewer lipid droplets on electron microscopy in the RPE compared to ApoM<sup>KO</sup> plasma-treated mice

(Fig. 1D–F). A decrease in number of lipid droplets was also associated with significantly increased RPE melanosomes in ApoM<sup>TG</sup> plasma-treated mice (Fig. 1G). As melanosomes have been reported to be related to lysosomal function<sup>44–46</sup>, we hypothesized that ApoM could be reducing RPE lipotoxicity through lysosome-mediated lipid catabolism.

### ApoM plasma transfer improves rod photoreceptor function in high-fat diet-fed *Abca1/gt1<sup>rod/rod</sup>* mice

As described above, we have previously demonstrated that RPE dysfunction in *Abca1/gt1<sup>rod/rod</sup>* is associated with secondary rod photoreceptor dysfunction<sup>26,28</sup>. We further hypothesized that ApoM plasma transfer may improve rod photoreceptor function as rod photoreceptor function is closely tied to RPE function<sup>49</sup>. To measure rod photoreceptor function, we utilized full-field scotopic electroretinography to measure both the a-wave and b-wave amplitudes, which measure rod photoreceptor and inner retina function respectively<sup>50</sup> (Fig. 1H–J). Scotopic a-wave amplitudes were significantly improved in ApoM<sup>TG</sup> treated mice compared to ApoM<sup>KO</sup> plasma-treated mice. These findings demonstrate that ApoM<sup>TG</sup> plasma-treated mice demonstrate both improved RPE and rod photoreceptor function.

### SIP binding to ApoM is necessary for reduced RPE lipid accumulation and improved rod photoreceptor function

ApoM is the primary carrier of SIP<sup>32</sup>. We hypothesized that SIP binding to ApoM is necessary for the structural and functional rod photoreceptor and RPE improvement seen in Fig. 1. To test this, we obtained plasma from control mice (ApoM<sup>Ctrl</sup>) and mice with a triple mutation in the ApoM binding site for SIP (ApoM<sup>TM</sup>)<sup>40</sup>. ApoM<sup>TM</sup> produces a mutated ApoM that is unable to bind SIP. We then utilized a similar treatment paradigm (Fig. 1B) to test if ApoM defective for SIP binding rescues the rod and RPE phenotype seen in the *Abca1/gt1<sup>rod/rod</sup>* model (Fig. 2A). In contrast to what we observed with ApoM plasma transfer, full-field scotopic electroretinography revealed reduced scotopic a-wave and b-wave amplitudes in ApoM<sup>TM</sup>-treated mice (Fig. 2B–D). Thus, mutated ApoM could not functionally improve rod photoreceptors as wild-type ApoM did in *Abca1/gt1<sup>rod/rod</sup>*.

We also assessed the ultrastructural effects of ApoM<sup>TM</sup> plasma transfer by electron microscopy. We quantified lipid droplet and melanosome counts within the RPE (Fig. 2E and F) through electron microscopy analysis. Corroborating the phenotype seen in rod photoreceptors, we appreciated significantly increased lipid droplet counts in the ApoM<sup>TM</sup> treated RPE compared to those of ApoM<sup>Ctrl</sup> treated RPE, despite similar melanosome counts (Fig. 2G and H). These data support that functional ApoM binding to SIP is necessary for the reduction of RPE lipid burden and functional preservation of rod photoreceptors.

### SIP receptor 3 knockout mice demonstrate RPE lipotoxicity and visual dysfunction

We next hypothesized which SIP receptor could be mediating RPE lipid amelioration in AMD-like phenotypes. Using publicly available bulk RNA sequencing data of human RPE cells (Supplementary Fig. 1)<sup>51</sup>, we identified that two of the five SIP receptors, SIP receptor 1 (SIPR1) and SIP receptor 3 (SIPR3), were the predominantly expressed receptors. We first generated conditional RPE knockout mice of *Sipr1* (*Sipr1<sup>RPE/RPE</sup>*) and placed them on a six week high fat diet to discern whether they phenocopy high fat diet fed *Abca1/gt1<sup>rod/rod</sup>* mice (Supplementary Fig. 2A). We did not see any RPE or rod photoreceptor dysfunction in knockout mice compared to wild type controls (Supplementary Fig. 2B–2D).

In-situ hybridization data of *Sipr3* expression in the eye demonstrated that *Sipr3* is expressed in the RPE (Supplementary Fig. 3). We assessed germline *Sipr3* knockout mice (*Sipr3<sup>-/-</sup>*) to

determine if they develop RPE lipotoxicity after six weeks of high-fat diet (Fig. 3A) treatment. Light bleach dark adaptation electroretinography assessment of *Sipr3<sup>-/-</sup>* RPE demonstrated significantly reduced RPE function compared to that of wild type RPE (Fig. 3B). Electron microscopy assessment of RPE ultrastructure demonstrated strikingly similar characteristics of high fat diet fed *Abca1/gt1<sup>rod/rod</sup>* RPE (Fig. 3C and D). Lipid droplet and melanosome quantification of *Sipr3<sup>-/-</sup>* RPE showed significantly increased lipid droplet count and decreased melanosome count (Fig. 3E and F) compared to those of wild-types. Full field scotopic electroretinography also showed significantly decreased scotopic a-wave amplitudes in *Sipr3<sup>-/-</sup>* (Fig. 3G–I) compared to wild-types. These data suggest that SIPR3 loss-of-function recapitulates the characteristic features of RPE lipotoxicity seen in the *Abca1/gt1<sup>rod/rod</sup>* model.

### Overexpression of ApoM does not rescue high-fat diet-induced *Sipr3<sup>-/-</sup>* RPE lipotoxicity

We next sought to investigate if ApoM can rescue the high fat diet-induced *Sipr3<sup>-/-</sup>* RPE lipotoxicity phenotype. We generated *Sipr3<sup>-/-</sup>/ApoM<sup>TG</sup>* mice and placed them on a 6-week high fat diet (Fig. 4A). No significant differences were appreciated in RPE function as measured by light bleach dark adaptation electroretinography between *Sipr3<sup>-/-</sup>* and *Sipr3<sup>-/-</sup>/ApoM<sup>TG</sup>* (Fig. 4B). Ultrastructural analysis of RPE through electron microscopy demonstrated similar features between *Sipr3<sup>-/-</sup>* and *Sipr3<sup>-/-</sup>/ApoM<sup>TG</sup>* (Fig. 4C and D). No significant differences were found between *Sipr3<sup>-/-</sup>* and *Sipr3<sup>-/-</sup>/ApoM<sup>TG</sup>* in lipid droplet quantification (Fig. 4E). Full-field scotopic electroretinography also did not show significant differences between *Sipr3<sup>-/-</sup>* and *Sipr3<sup>-/-</sup>/ApoM<sup>TG</sup>* in scotopic a-wave and b-wave amplitudes (Fig. 4F–H). These data suggest SIPR3 is necessary for ApoM-SIP alleviate RPE lipid burden and associated visual dysfunction.

### ApoM-SIP-mediated clearance of photoreceptor outer segment lipids by RPE requires SIPR3

In the eye, there is a diurnal rhythm associated with the shedding of photoreceptor outer segments (POS). There is extensive shedding of rod outer segments at dawn, while cones shed at dusk. This creates a large lipid burden for the RPE to phagocytose and metabolize daily over the lifetime of the organism<sup>52–54</sup>. To elucidate RPE lipotoxicity mechanisms, we sought to emulate the POS clearance by RPE cells in vitro and ex vivo. We utilized ARPE-19 cells to simulate the lipid burden seen in the in vivo genetic model exacerbated by the high-fat diet. We accomplished this by treating ARPE-19 cells with exogenous photoreceptor outer segments at varying concentrations (Supplementary Fig. 4). This model has been extensively characterized to test RPE phagocytic and lipid processing capacity<sup>44,45,55,56</sup>. Using commercially available bovine POS, we first visualized if ARPE-19 cells would fluoresce with increasing intensity when treated with FITC-labeled POS (Supplementary Fig. 4A). We treated cells with no POS, or at a 10:1, or 20:1 POS to RPE cell ratio. Cells were treated with POS for 4 hours before fixing and imaging. Indeed, the ARPE-19 cells demonstrated increased intensity of fluorescence according to the concentration of FITC-labeled POS. We then sought to appreciate the amount of neutral lipid through BODIPY staining after POS treatment of RPE cells at a 10:1 and 20:1 POS to RPE ratio (Supplementary Fig. 4B). Cells were treated with POS for 4 hours before fixing and imaging. The 10:1 POS to RPE ratio is typically used to observe baseline phagocytic and processing behavior of RPE<sup>55</sup>. Indeed, we observed that increased POS feeding led to increased BODIPY staining. We next tested if recombinant ApoM loaded with SIP could decrease BODIPY staining after POS feeding. To test this, we incubated the cells with media containing recombinant ApoM loaded with SIP (25 µg/mL) for an additional 2 hours after 4 hours of POS treatment. We observed reduced BODIPY staining within RPE cells treated with POS after incubation with ApoM-SIP compared to controls that did not receive ApoM-SIP in the medium.

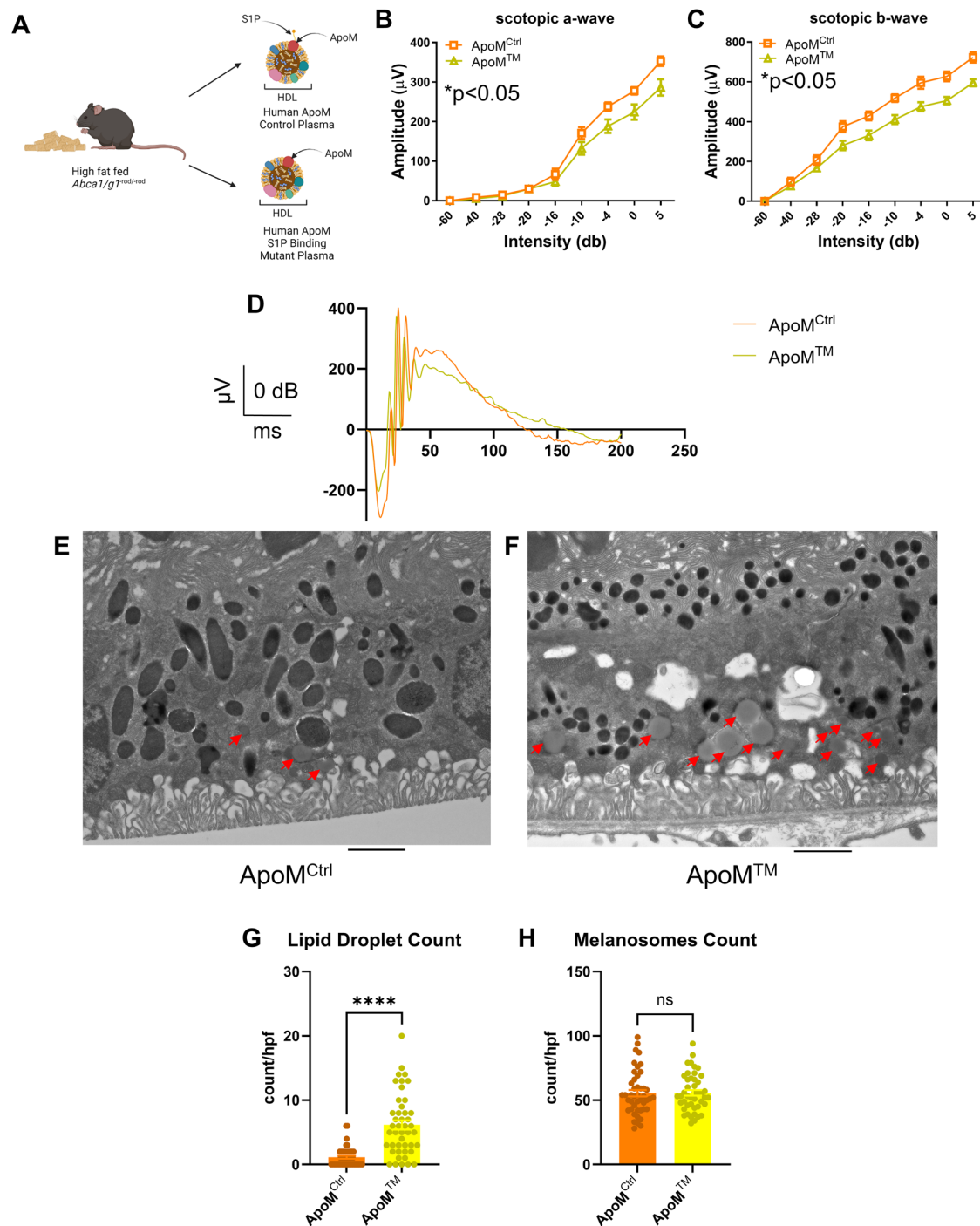


**Fig. 2 | Binding of SIP by ApoM is necessary for RPE lipotoxicity amelioration.**

**A** High fat diet fed *Abca1/g1<sup>rod/rod</sup>* were treated with plasma from either control mice with human ApoM knocked in (ApoM<sup>Ctrl</sup>) or mice expressing ApoM incapable of binding SIP (ApoM<sup>TM</sup>) (created in BioRender. Lee, T. (2025) <https://BioRender.com/li4w1zf>). Full-field scotopic electroretinography ( $n = 4$ ) demonstrated significant reduction in **B** rod photoreceptor ( $*p = 0.0469$ , Two-way ANOVA) and **C** inner retina function ( $*p < 0.0199$ , Two-way ANOVA) in ApoM<sup>TM</sup> treated mice. **D** Representative traces of 0 dB intensity flashes show the waveform from ApoM<sup>TM</sup> treated mice do not recover. **E, F** Representative TEM imaging of RPE from either

ApoM<sup>Ctrl</sup> or ApoM<sup>TM</sup> plasma treated *Abca1/g1<sup>rod/rod</sup>* mice. Red arrows point to lipid droplets. **G** Quantitative assessment of lipid droplets per high-powered field within the RPE ( $n = 45$ ) revealed significantly increased lipid droplets in ApoM<sup>TM</sup> plasma treated mice ( $****p < 0.000000013$ , two-tailed Welch's t-test). **H** Quantitative assessment of melanosomes per high-powered field within the RPE ( $n = 45$ ) revealed no significant difference according to two-tailed Welch's t-test without multiple comparisons in melanosome counts between ApoM<sup>Ctrl</sup> and ApoM<sup>TM</sup> plasma treated mice. Scale bar represents 2  $\mu\text{m}$ . Values are mean  $\pm$  SE. Source data are provided as a Source Data file.

These data suggest in vitro ARPE-19 cells respond similarly to ApoM-SIP as in vivo RPE do.

We further sought to test and quantify the effect of POS treatment on RPE cells in an ex vivo 'eyecup' system (Fig. 5A). We dissected RPE, choroid, and sclera complex from wild-type mice to

compose the ex vivo 'eyecup' system. We then incubated the eyecup with different amounts of POS, then subsequently incubated the eyecups with control media or media with recombinant ApoM-SIP. Eyecups were treated with POS for two hours and then treated with ApoM-SIP for two hours<sup>55</sup>. We calculated the amount of POS

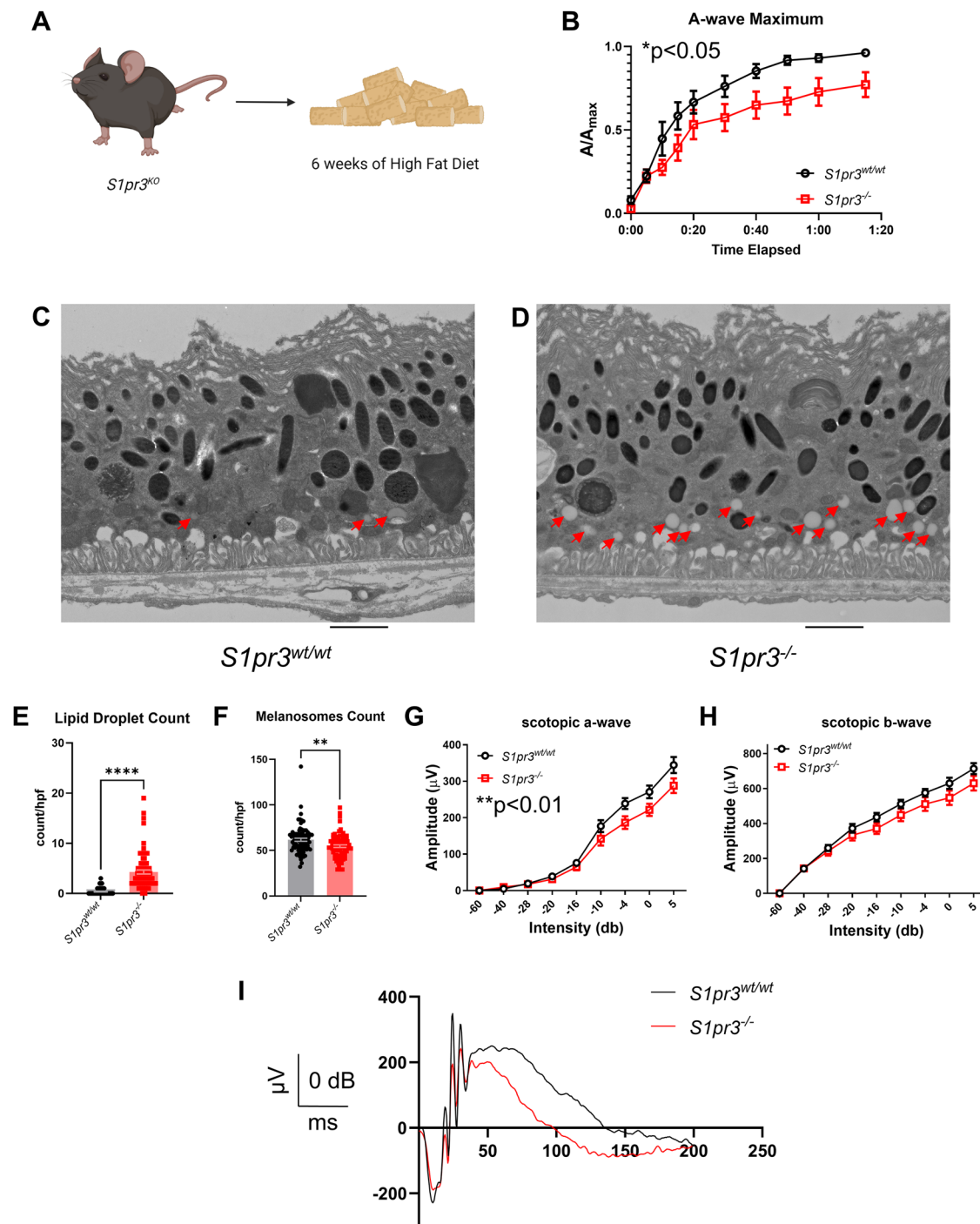


**Fig. 3 | *S1pr3* knockout is sufficient to provoke a dry AMD-like RPE phenotype.**

**A** *S1pr3* germline knockout mice (*S1pr3*<sup>-/-</sup>) were generated and placed on 6 weeks of high fat diet and subsequently assessed (created in BioRender. Lee, T. (2025) <https://BioRender.com/li4w1zf>). **B** RPE functional assessment using light bleach dark adaptation electroretinography ( $n = 10$ ) revealed significantly reduced functional recovery in *S1pr3*<sup>-/-</sup> mice compared to wild-type mice ( $*p = 0.0462$ , Two-way ANOVA). **C, D** Representative TEM imaging of RPE from either wild-type or *S1pr3* knockout mice. Red arrows point to lipid droplets. **E** Quantitative assessment of lipid droplets per high-powered field within the RPE ( $n = 80$ ) revealed significantly

increased lipid droplets in *S1pr3* knockout mice ( $****p = 0.000000001$ , two-tailed Welch's t-test). **F** Quantitative assessment of melanosomes per high-powered field within the RPE ( $n = 80$ ) revealed significantly decreased melanosomes in *S1pr3* knockout mice ( $**p = 0.0018$ , two-tailed Welch's t-test). Full-field scotopic electroretinography ( $n = 8$ ) demonstrated reduced **G** rod photoreceptor ( $**p = 0.0018$ , Two-way ANOVA) but not **H** inner retina (Two-way ANOVA) function in *S1pr3* knockout mice. **I** Representative traces of 0 dB intensity flashes show a diminutive waveform from *S1pr3*<sup>-/-</sup>. Scale bar represents 2  $\mu\text{m}$ . Values are mean  $\pm$  SE. Source data are provided as a Source Data file.

necessary for treatment according to a previous report quantifying approximate counts of RPE cells (25,000 cells in one eyecup) in mouse eyecups<sup>57</sup>. The eyecups were then stained with BODIPY, flat mounted, and imaged (Fig. 5B and C). Of note, eyecups treated with ApoM or SIP alone did not demonstrate a significant effect on

BODIPY fluorescence compared to ApoM-SIP, suggesting ApoM and SIP must be present together (Supplementary Fig. 5A and 5B).

We utilized the same experimental paradigm of lipid staining ex vivo eyecups from *S1pr3*<sup>-/-</sup> mice (Fig. 5D and E). BODIPY fluorescence was then quantified across multiple images (Fig. 5F). Wild-type

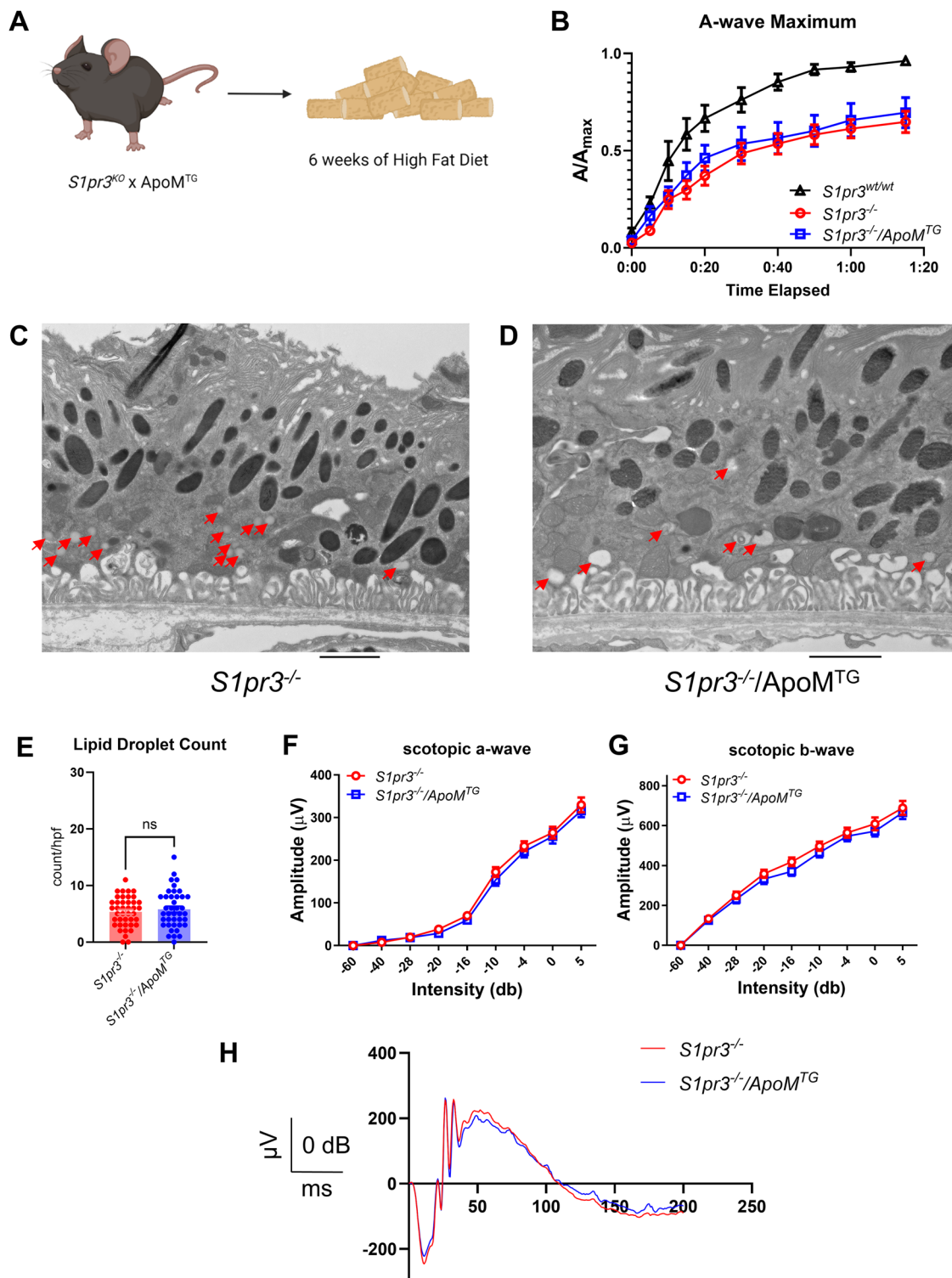


**Fig. 4 | ApoM overexpression does not rescue S1PR3 deficiency-induced RPE lipotoxicity.** **A** *S1pr3* germline knockout mice (*S1pr3<sup>-/-</sup>*) were crossed with ApoM overexpressing transgenic mice (*ApoM<sup>TG</sup>*) to generate *S1pr3<sup>-/-</sup>/ApoM<sup>TG</sup>* mice and placed on 6 weeks of high fat diet and subsequently assessed (created in BioRender. Lee, T. (2025) <https://BioRender.com/li4w1zlf>). **B** RPE functional assessment using light bleach dark adaptation electroretinography ( $n = 6$ ) revealed no significant differences in functional recovery between *S1pr3<sup>-/-</sup>* and *S1pr3<sup>-/-</sup>/ApoM<sup>TG</sup>* mice. **C, D** Representative TEM imaging of RPE from either *S1pr3<sup>-/-</sup>* or *S1pr3<sup>-/-</sup>/ApoM<sup>TG</sup>* mice. Red arrows point to lipid droplets. **E** Quantitative assessment of lipid droplets

per high-powered field within the RPE ( $n = 42$ ) revealed no significant differences using two-tailed Welch's t-test without multiple comparisons between *S1pr3<sup>-/-</sup>* and *S1pr3<sup>-/-</sup>/ApoM<sup>TG</sup>* mice. Full-field scotopic electroretinography ( $n = 8$ ) demonstrated no significant differences by two-way ANOVA in **F** rod photoreceptor and **G** inner retina between *S1pr3<sup>-/-</sup>* and *S1pr3<sup>-/-</sup>/ApoM<sup>TG</sup>* mice. **H** Representative traces of 0 dB intensity flashes show waveforms do not improve despite ApoM<sup>TG</sup> treatment in *S1pr3<sup>-/-</sup>*. Scale bar represents 2  $\mu$ m. Values are mean  $\pm$  SE. Source data is provided as a Source Data file.

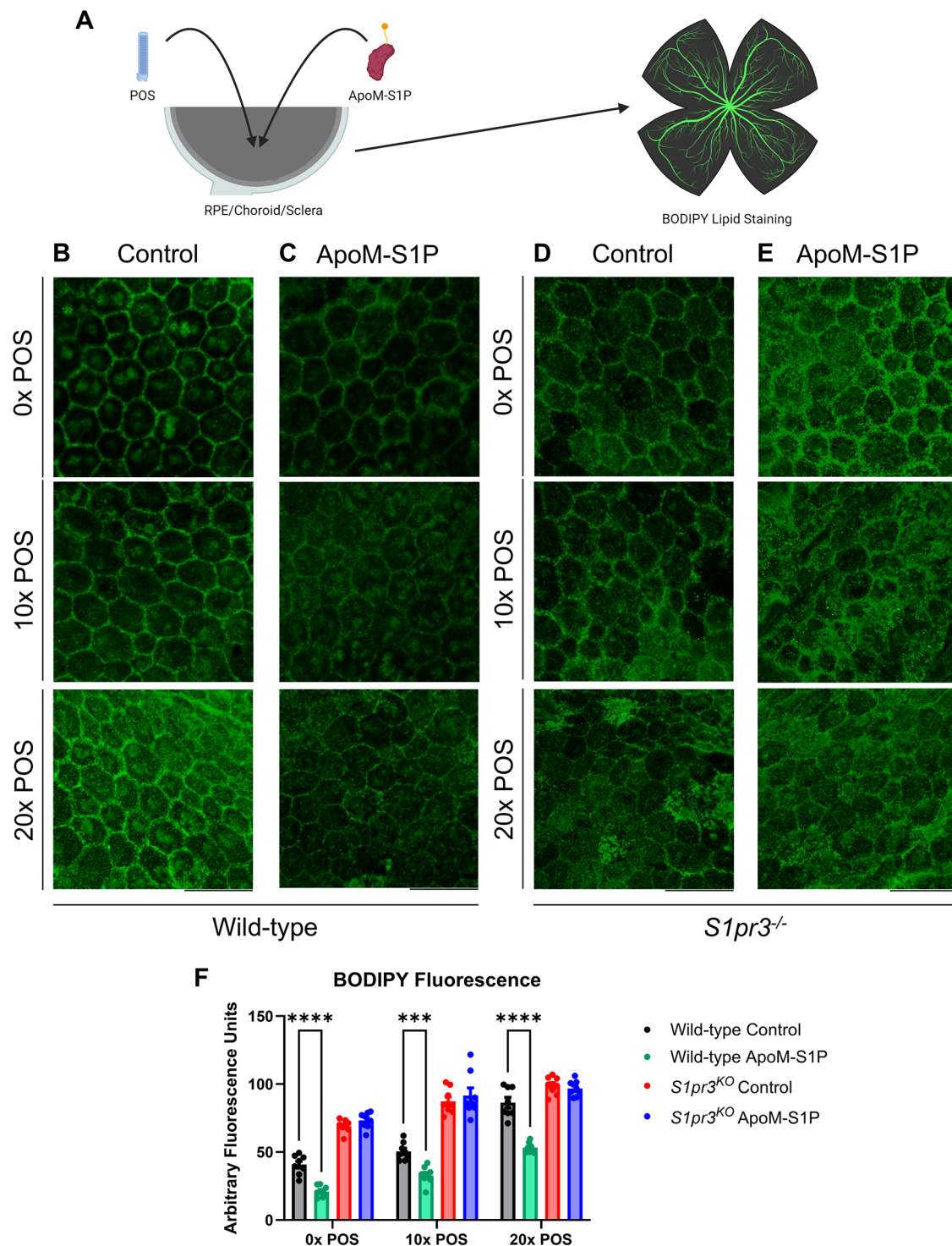


**Fig. 5 | RPE from ex vivo eyecups recapitulate in vivo lipid burden.** **A** The RPE/choroid/sclera complex was isolated from mouse eyecups to assess ex vivo RPE for lipid burden using BODIPY neutral lipid staining depicted in green (created in BioRender. Lee, T. (2025) <https://BioRender.com/li4w1zf>). Eyecups from wild-type mice were treated with increasing dosages of photoreceptor outer segments (POS) before being treated with either **B** control media or **C** media with ApoM-S1P. The same paradigm was tested in eyecups from *S1pr3<sup>-/-</sup>* mice also treated with either **D** control media or **E** media with ApoM-S1P. **F** BODIPY fluorescence was quantified from each group and plotted ( $n = 8$ ). Wild-type RPE treated with ApoM-S1P

expressed significantly less BODIPY fluorescence compared to those treated with control media in 0x ( $****p = 0.000022$ , post hoc Bonferroni's multiple comparisons test), 10x ( $***p = 0.00017$ , post hoc Bonferroni's multiple comparisons test), and 20x POS ( $****p = 0.0000000001$ , post hoc Bonferroni's multiple comparisons test) treated groups ( $****p = 0.0000000001$ , Two-way ANOVA). ApoM-S1P treated *S1pr3<sup>KO</sup>* RPE did not demonstrate significant differences in BODIPY fluorescence compared to control-treated *S1pr3<sup>KO</sup>* RPE. The scale bar represents 100  $\mu\text{m}$ . Values are mean  $\pm$  SE. Source data is provided as a Source Data file.

RPE treated with ApoM-SIP demonstrated significantly reduced BODIPY fluorescence compared to those treated with control media in 0x, 10x, and 20x POS treated groups. However, ApoM-SIP treatment did not significantly change BODIPY fluorescence in *S1pr3*<sup>-/-</sup> RPE. Consistent with our *in vivo* models, these data show ApoM-SIP does not reduce the amount of lipid staining in *S1pr3*<sup>-/-</sup> RPE, suggesting that ApoM-SIP requires functional S1PR3 to ameliorate RPE lipid burden. These data support the conclusions from the *in vivo* genetic and pharmacologic experiments presented above that ApoM-SIP helps reduce lipid burden in wild-type RPE, and S1PR3 function is necessary for adequate lipid processing from POS.

### ApoM-SIP does not significantly improve cholesterol efflux capacity in RPE cells

After characterizing the effects of ApoM-SIP on RPE lipotoxicity, we investigated the mechanism of the effect of ApoM-SIP on the lipotoxicity phenotype, utilizing ARPE-19 cells. We performed *in vitro* administration of ApoM-SIP<sup>41</sup> to measure total cholesterol efflux capacity from ARPE-19 cells (Supplementary Fig. 6). Serum from ApoM knockout mice was used as cholesterol acceptors for the assay. Although previous studies suggest ApoM influences macrophage cholesterol efflux<sup>43</sup>, ApoM-SIP did not significantly affect cholesterol efflux capacity in ARPE-19 cells. These data suggest that ApoM-SIP does not reduce RPE lipid burden through cholesterol efflux, and ApoM-SIP influences cholesterol efflux in a cell-type-dependent manner.

### Lipophagy knockout induces RPE lipotoxicity features

Based on our observations of increased melanosome counts with ApoM treatment in *Abca1/gli1<sup>rod/rod</sup>*, enhanced lysosomal lipid catabolism was a suspected mechanism of ApoM-SIP mediated lipid burden amelioration as melanosome and lysosomal function have been closely associated<sup>44–46</sup>. Previous work has demonstrated that ApoM is a novel regulator of autophagy and that ApoM preserves lysosomal function<sup>40</sup>. We therefore hypothesized that abrogating lysosomal lipid catabolism would recapitulate features of RPE lipotoxicity.

Lysosomal acid lipase (LAL; gene name *Lipa*) is a critical enzyme that is necessary for lysosomal lipid catabolism<sup>58,59</sup>. We generated germline LAL knockout mice (*Lipa*<sup>-/-</sup>) and placed them on high fat diet to investigate if abrogation of lysosomal lipid catabolism leads to AMD-like phenotypes (Supplementary Fig. 7A). Ultrastructural analyses of RPE demonstrated intracellular lipid droplets that are improperly processed in *Lipa*<sup>-/-</sup> mice (Supplementary Fig. 7B and 7C). Light bleach dark adaptation electroretinography of *Lipa*<sup>-/-</sup> mice showed decreased RPE function (Supplementary Fig. 7D). Full field scotopic electroretinography demonstrated significantly reduced rod photoreceptor function in *Lipa*<sup>-/-</sup> (Supplementary Fig. 7E and 7F). Since LAL is ubiquitously expressed, lack of LAL most likely caused severe effects in all cell types, including photoreceptors.

To pinpoint the role of lysosomal lipid catabolism in RPE, we generated a *Lipa* conditional RPE knockout (*Lipa*<sup>RPE/RPE</sup>)<sup>60</sup> and placed them on high fat diet (Fig. 6A). *Lipa*<sup>RPE/RPE</sup> mice demonstrated significantly reduced RPE function by light bleach dark adaptation electroretinography (Fig. 6B). Ultrastructural analyses by electron microscopy of RPE cells showed a significant increase in lipid droplets in the RPE of *Lipa*<sup>RPE/RPE</sup> (Fig. 6C). Representative images demonstrate increased lipid droplet accumulation in RPE cells of *Lipa*<sup>RPE/RPE</sup> compared to controls (Fig. 6D and E). However, no significant differences were appreciated in rod photoreceptor function by full field scotopic electroretinography (Supplementary Fig. 8A and 8B).

### ApoM plasma transfer therapy does not rescue *Lipa* knockout-induced RPE lipotoxicity

To test if ApoM can rescue RPE lipotoxicity in *Lipa*<sup>RPE/RPE</sup>, we utilized ApoM plasma transfer, as performed in Fig. 1C (Fig. 6F). Functional

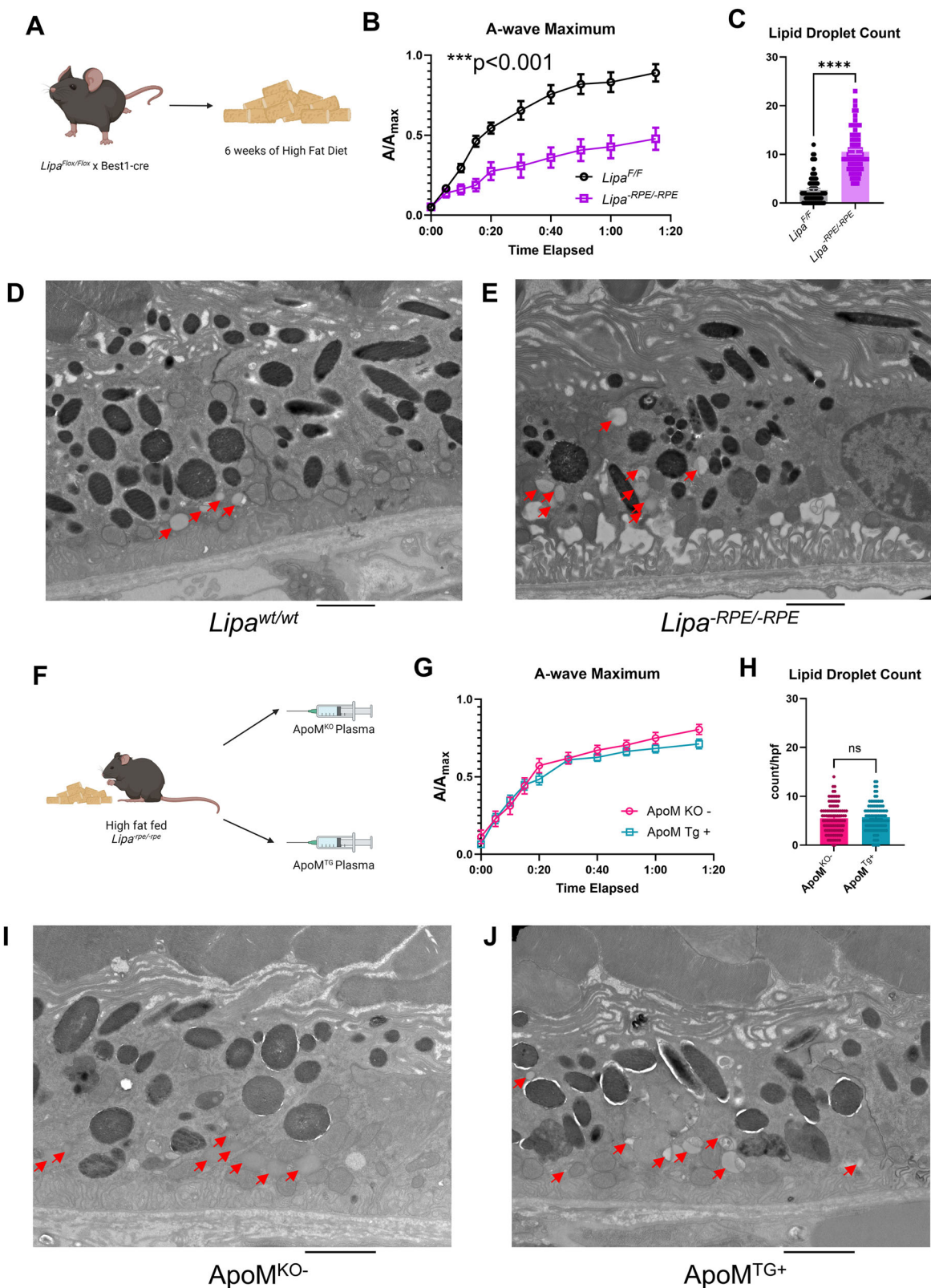
assessment of RPE and rod photoreceptor function demonstrated no significant differences between the two groups (Fig. 6G) (Supplementary Fig. 8C and 8D). Quantification of lipid droplet count by TEM demonstrated no significant differences between groups (Fig. 6H–J). These results suggest that ApoM attenuates RPE lipotoxicity through LAL. Consistent with this effect, we performed *in vitro* studies in ARPE-19 cells to test the hypothesis that LAL acts downstream of ApoM-SIP signaling. We treated ARPE-19 cells with Lalistat-2 in the presence of ApoM-SIP and examined BODIPY fluorescence after POS treatment (Supplementary Fig. 9). ARPE-19 cells were first treated with POS, then either with ApoM-SIP alone or ApoM-SIP with Lalistat-2, an inhibitor of LAL, then mounted and stained for neutral lipids using BODIPY staining (Supplementary Fig. 9A). Fluorescence intensities were subsequently quantified and analyzed (Supplementary Fig. 9B). Both groups exhibited increased fluorescence with higher doses of POS. Furthermore, cells treated with Lalistat-2 displayed significantly more fluorescence than those not treated with Lalistat-2, despite ApoM-SIP treatment. In aggregate, these results are consistent with LAL acting downstream of ApoM-SIP to reduce RPE lipid burden.

## Discussion

In this study, we identified a novel role for the lipocalin ApoM in RPE lipotoxicity as seen in early dry AMD and recapitulated in murine models (Fig. 7). We discovered that patients with AMD had significantly reduced circulating ApoM, as measured by ELISA. We demonstrated that several pathogenic features observed in murine models of dry AMD, such as RPE and rod photoreceptor dysfunction and RPE lipid accumulation, are improved by ApoM. We also demonstrated that the salutary effects of ApoM are contingent on SIP binding. Furthermore, we identified S1PR3 as a critical target of ApoM-SIP as *S1pr3* knockout recapitulated dry AMD-like features. While ApoM-SIP reduced the lipid burden of the RPE as seen in the *ex vivo* eye cup assay, this effect required S1PR3. Finally, we identified a cell-autonomous role for LAL in the RPE, as not only did the RPE-specific LAL knockout develop AMD-like features, but it was not rescued by ApoM therapy. In totality, our studies identify a novel role for ApoM in AMD pathogenesis through RPE lipotoxicity, ApoM/SIP/S1PR3 signaling, and LAL.

As existing therapies for AMD are tailored towards the advanced stages, we endeavored to explore new therapeutic avenues for the early to intermediate forms of AMD. Utilizing the high fat diet fed *Abca1/gli1<sup>rod/rod</sup>* model, we highlighted the RPE's limitations of processing improperly loaded photoreceptor outer segments that lead to lipotoxicity reminiscent of early to intermediate AMD. As *ABCA1* polymorphisms are a characterized risk factor for AMD<sup>21</sup>, we believe this is a reasonable model that recapitulates several features of early AMD<sup>26</sup>. RPE lipotoxicity is a key driver of AMD pathogenesis and progression, underscoring the urgent need for innovative strategies to reduce lipid accumulation in the RPE and associated sub-retinal and sub-RPE regions. The RPE relies primarily on two mechanisms for lipid clearance: efflux and catabolism<sup>56,58,61</sup>. While ApoM and SIP are known to facilitate cholesterol transport in other cell types, our data show that recombinant ApoM-SIP does not significantly enhance cholesterol efflux in ARPE-19 cells. This led us to explore and alternative role for ApoM in promoting lipid catabolism within the RPE. Our observations, particularly the changes in melanosome and lipid droplet numbers following ApoM plasma transfer, suggest ApoM may enhance lysosomal lipid catabolism. This study as a whole supports the notion that ApoM-SIP signaling upregulates lysosomal acid lipase activity, a mechanism that warrants further investigation.

Our study also establishes a novel role for S1PR3 in AMD pathogenesis in the mouse. While bulk RNA sequencing of human RPE indicates that *S1PR1* and *S1PR3* are the predominantly expressed SIP receptors, previous investigations have identified other SIP receptors, such as *S1PR2*, play an essential role in RPE function<sup>41</sup>. Notably, Terao et al. demonstrated that S1PR2 modulates the inflammatory profile of



ARPE-19 cells, and intravitreal administration of a selective S1PR2 inhibitor significantly reduced lesion size in a laser-induced choroidal neovascularization (CNV) model. These findings implicate S1PR2 in the regulation of inflammatory and angiogenic pathways in the RPE and potentially other cell types involved in CNV. Although *S1PR4* and *S1PR5* are expressed at low levels in RPE, their roles along with that of S1PR2 should be further explored in early-stage dry AMD models to better understand their contributions to disease mechanisms.

It is evident that AMD pathogenesis is complex and influenced by numerous genetic and environmental factors, in addition to the effects of aging on the eye. As such, it is critical to identify and target the earliest triggers of disease pathogenesis prior to catastrophic vision loss. Our study, specifically focused on addressing the fundamental mechanisms of RPE lipotoxicity, highlights a novel therapeutic use of ApoM-SIP to prevent RPE lipotoxicity via enhanced elimination of lipids and deserves further exploration.

**Fig. 6 | RPE-specific knockout of lipophagy recapitulate features of a dry AMD-like phenotype.** **A** RPE-specific lysosomal acid lipase conditional knockout mice ( $Lipa^{RPE/RPE}$ ) were generated and placed on 6 weeks of high fat diet and subsequently assessed (created in BioRender. Lee, T. (2025) <https://BioRender.com/li4w1zf>). **B** RPE functional assessment using light bleach dark adaptation electroretinography ( $n = 6$ ) revealed significantly reduced functional recovery in  $Lipa^{RPE/RPE}$  mice compared to wild-type mice ( $***p = 0.000468$ , Two-way ANOVA). **C** Quantitative assessment of lipid droplets per high-powered field within the RPE ( $n = 76$ ) revealed significantly increased lipid droplets in  $Lipa^{RPE/RPE}$  mice ( $****p = 0.0000000001$ , two-tailed Welch's t-test). **D, E** Representative TEM imaging of RPE from either wild-type or  $Lipa^{RPE/RPE}$

mice. Red arrows point to lipid droplets. **F** High fat diet fed  $Lipa^{RPE/RPE}$  mice were treated with either ApoM<sup>KO</sup> or ApoM<sup>TG</sup> plasma (created in BioRender. Lee, T. (2025) <https://BioRender.com/li4w1zf>). **G** RPE functional assessment using light bleach dark adaptation electroretinography ( $n = 6$ ) revealed no significant differences by two-way ANOVA in functional recovery. **H** Quantitative assessment of lipid droplets per high-powered field within the RPE ( $n = 100$ ) revealed no significant differences according to two-tailed Welch's t-test without multiple comparisons in lipid droplet counts. **I, J** Representative TEM imaging of RPE from either wild-type or  $Lipa^{RPE/RPE}$  mice. Red arrows point to lipid droplets. The scale bar represents 2  $\mu\text{m}$ . Values are mean  $\pm$  SE. Source data is provided as a Source Data file.

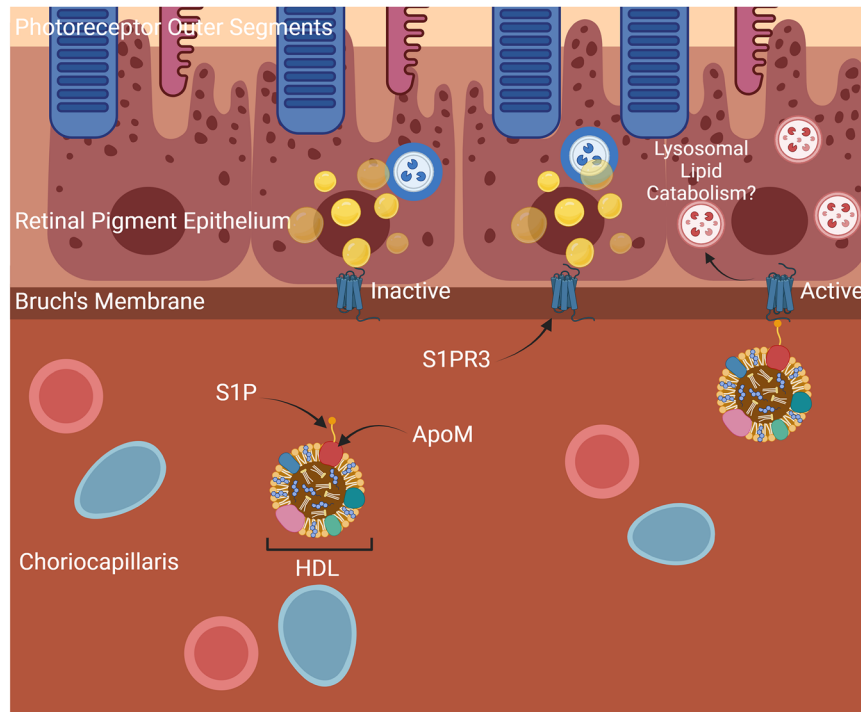


**Fig. 7 | ApoM-SIP as a potential therapeutic for early dry AMD.** ApoM is carried by HDL particles in systemic circulation and is made available to the RPE through the choriocapillaris. ApoM and its binding partner, SIP, activates S1PR3 on the RPE surface to activate lysosomal lipid catabolism to alleviate RPE lipid burden. Inactive S1PR3 allows aberrant accumulation of intracellular lipids within the RPE, leading to

dysfunction and potentially increasing the risk to develop dry AMD features. By supplying the RPE with exogenous ApoM-SIP through plasma transfer, we can reduce lipid burden in the RPE through a S1PR3-dependent mechanism and subsequently reduce the risk of dry AMD pathogenesis (created in BioRender. Lee, T. (2025) <https://BioRender.com/li4w1zf>).

## Methods

### Animals

All animal experiments were conducted in accordance with the ARVO Statement for the Use of Animals in Ophthalmic and Vision Research and Washington University School of Medicine in St. Louis Animal Care and Use guidelines and after approval by the Institutional Animal Care and Use Committee (IACUC). Animals were monitored daily and euthanized by CO<sub>2</sub> at experiment endpoints according to these guidelines. All animal experiments abide by the ARRIVE guidelines. Male and female mice between 8 and 12 weeks old (2-3 months of age) were used in this study. Mice were housed in a 12-hour light/dark cycle with free access to food and water. For high fat diet (HFD) feeding experiments, only male mice were used. We used an adjusted-calorie diet (60% from fat, 25% kcal from carbohydrate, and 15% kcal from protein (ENVIGO, Indianapolis, IN) as HFD, starting from 6 weeks old to the target age of analysis. We used Purina 4043 chow (13% kcal from fat, 62% kcal from carbohydrate, 25% kcal from protein) as the normal diet.  $ApoM^{KO}$ <sup>37</sup>,  $ApoM^{TG}$ <sup>35,40</sup>,  $S1pr3^{-/-}$ <sup>62</sup>, and  $S1pr1^{RPE/RPE}$ <sup>63</sup> have been described in previous studies and generated in house.  $Lipa^{-/-}$  and  $Lipa^{RPE/RPE}$  mice were donated by Drs. Jaya

Mishra (University of Cincinnati College of Medicine) and Dagmar Kratky (Gottfried Schatz Research Center) respectively and generated in house<sup>60,64</sup>. Mice with RPE conditional knockouts were crossed with mice carrying one copy of the Bestrophin1 (Best1-cre) transgene, which are available from Jackson Laboratories (017557). Mice were fully backcrossed to the inbred C57BL/6J background.

### Human dataset

Generation of the human dataset was approved by the Human Research Protection Office of Washington University School of Medicine in St. Louis and the study was conducted according to the Declaration of Helsinki and approved by Danish Ethics committees (no. KF-100.2039/91, KF-01-144/01, H-KF-01-144/01) and the Washington University in St. Louis Institutional Review Board (IRB#201301075). We obtained written informed consent from all patients prior to enrollment in the study. Patients were not excluded based on gender, sex, race, ethnicity, or other socially relevant groupings. We classified samples as coming from patients with no AMD; early AMD; or AMD with geographic atrophy and/or CNV based on established clinical criteria. Early AMD patients had either small or moderate drusen (< 125

µm) or pigment changes in at least 1 eye but no CNV or geographic atrophy in either eye. Patients with geographic atrophy and/or CNV in at least 1 eye were labeled as such. We excluded any patients receiving immunotherapy, chemotherapy, or radiation for underlying autoimmune/immune-mediated diseases or cancers, which could affect circulating immune cells.

### Sandwich ELISA for human unfolded plasma ApoM

We obtained informed consent from patients with dry or wet AMD and collected blood via venous blood draw into K<sub>2</sub>EDTA-coated BD Vacutainer Venous Blood Collection Tubes. Samples were then deidentified. Plasma was separated and collected after centrifugation. An ELISA plate (Costar 3590 high binding) was coated with 50 µl of capture antibody (clone 1G9) by diluting to 5 µg/ml in TBS (pH 7.4) and incubated at room temperature overnight. The plate was blocked for 2 h with 200 µl of 2% BSA in TBS (pH 7.4). Ten microliters of each plasma sample were mixed with 90 µl of 50 mmol/l DTT (Sigma-Aldrich) in a 0.2 mol/l sodium phosphate buffer (pH 8.5). Disulfide bridges in ApoM were broken by incubating samples at 30 °C for 15 min. One hundred microliters of 0.6 mol/l iodoacetamide (Sigma-Aldrich) in a 0.02 mol/l sodium phosphate buffer (pH 8.0) were then added, and samples were incubated for 1 h at room temperature in the dark to alkylate free cysteines in ApoM and prevent reformation of disulfide bridges. After 1 h, the samples were diluted fifty times (variable for the standard curve) in TBS (pH 7.4) containing 1% BSA and transferred to the ELISA plate for overnight incubation at room temperature. The plate was washed three times with TBS (pH 7.4) and incubated overnight at room temperature with 75 µl of detection antibody (clone EPR2904) diluted to 125 ng/ml in TBS (pH 7.4) containing 1% BSA and 2% Triton-X 100. The plate was washed three times with TBS (pH 7.4) and 0.1% Triton-X 100 and incubated for 2 h with 75 µl of HRP-conjugated anti-rabbit IgG antibody diluted to 125 ng/ml in TBS (pH 7.4) containing 1% BSA and 0.1% Triton-X 100. Finally, the plate was washed three times with TBS (pH 7.4) and 0.1% Triton-X 100, and ApoM was detected by reading absorbance at 492 nm after incubation with 75 µl o-phenylenediamine/hydrogen peroxide solution for 10 min followed immediately by addition of 75 µl 1 mol/l H<sub>2</sub>SO<sub>4</sub>. The ApoM concentration of measured samples was determined from the standard curve included in each assay run.

### Plasma transfer

Plasma was obtained from either *ApoM<sup>KO</sup>* or *ApoM<sup>TG</sup>* mice from peripheral blood via the retro-orbital plexus under anesthesia. 120 µl of either *ApoM<sup>KO</sup>* or *ApoM<sup>TG</sup>* plasma was intraperitoneally injected in *Abca1/gt<sup>rod/rod</sup>* starting at 6 weeks of age. High fat diet was implemented on the first day of injections. Mice were injected thrice weekly for 6 weeks.

### Electroretinography

Full field scotopic ERG was performed as previously described<sup>50</sup>. A UTAS BigShot System (LKC Technologies Inc.) was used. Mice were dark-adapted overnight. Under red light illumination, mice were anesthetized with an intraperitoneal injection of 86.9 mg/kg ketamine and 13.4 mg/kg xylazine. Pupils were dilated with 1% tropicamide eye drops. Body temperature was maintained at 37 °C with a heating pad. Contact lens electrodes were placed bilaterally with appropriate reference and ground electrodes. The stimulus consisted of a full-field white light flash (10 µs). Raw data were processed using MATLAB software (MathWorks). The *a* wave amplitude was measured from the average pretrial baseline to the most negative point of the average trace, and the *b* wave amplitude was measured from that point to the highest positive point.

For testing dark adaptation, we modified the protocol as previously described<sup>65</sup>. Briefly, we used a UTAS BigShot System (LKC

Technologies Inc.) to get scotopic a-waves. A bright LED light (150,000 lux) was applied to both eyes for 15 seconds to photobleach an estimated 90% of the visual pigment. The recovery of the ERG responses was monitored at fixed post-bleach time points within 100 minutes after the bleach. The sensitivity was calculated as the ratio of dim flash response amplitude and the corresponding flash intensity in the linear range of the intensity-response curve. The post-bleach sensitivities were normalized to their dark-adapted prebleach level.

### Transmission electron microscopy

We performed transmission electron microscopy as previously described<sup>50</sup>. For ultrastructural analyses, eyecups were fixed in 2% paraformaldehyde (PFA)/2.5% glutaraldehyde (Polysciences Inc.) in 100 mM sodium cacodylate buffer, pH 7.2, for 2 hours at room temperature and then overnight at 4 °C. Samples were washed in sodium cacodylate buffer at room temperature and postfixed in 1% osmium tetroxide (Polysciences Inc.) for 1 hour. Samples were then rinsed extensively in dH<sub>2</sub>O prior to en bloc staining with 1% aqueous uranyl acetate (Ted Pella Inc.) for 1 hour. Following several rinses in dH<sub>2</sub>O, samples were dehydrated in a graded series of ethanol and embedded in Eponate 12 resin (Ted Pella Inc.). Sections of 95 nm were cut with a Leica Ultracut UCT ultramicrotome (Leica Microsystems Inc.), stained with uranyl acetate and lead citrate, and viewed on a JEOL 1200 EX transmission electron microscope (JEOL USA Inc.) equipped with an AMT 8 megapixel digital camera and AMT Image Capture Engine V602 software (Advanced Microscopy Techniques).

### In-situ hybridization

RNAscope Multiplex Fluorescent V2 assay (ACDBio, Cat. No. 323100) was performed according to the manufacturer's instructions. Briefly, slides with ice cold 97% methanol/3% acidic acid-fixed, paraffin-embedded eye sections (4 µm thick) were baked for 60' at 60 °C before being deparaffinized in 2 changes of xylenes and dehydrated in two changes of 100% ethanol for 5' each, then fully dried in a 60 °C oven, -10'. Slides were then treated with RNAscope hydrogen peroxide solution for 10' at room temperature and washed twice in distilled water prior to 15' of antigen retrieval in 100 °C RNAscope target retrieval solution (ACDBio, Cat. No. 322000). After rinsing in distilled water, slides were dried in 100% Ethanol and placed in a 60 °C oven for 5'. Barriers were drawn around tissues using an ImmEdge hydrophobic Pen (Vector Labs, Cat. No. H-4000), and then slides were allowed to fully dry. All incubations were performed in a HybEZ oven (ACDBio, Cat. No. 241000ACD) at 40 °C. First, RNAscope Protease II solution was added to each slide for 30'. After 2 washes in nuclease-free water, probes were applied for 2 hr. MM-S1pr3 (ACDBIO, Cat. No. 435951), Mm-PPIB positive control (Cat. No. 313911) or negative control probes (Cat. No. 320871) were utilized on sequential sections from each eye. Following the kit's 3 amplification solution incubations at 37 °C and washes in RNAscope wash buffer (diluted to 1x in nuclease-free water), HRP-C1 solution was applied for 15' at 40 °C, followed by 2 changes of wash buffer and application of Opal 520 (Akoya Biosciences, Cat. No. FP1478001KT) diluted 1:1500 in TSA buffer for 30' at 40 °C. Slides were washed, nuclei were stained DAPI for 10' at room temp, washed in wash buffer two times and cover slipped using FluoroSave Reagent (Millipore-Sigma, Cat. No. 345789).

### Cell culture

ARPE-19 (CAT#CRL-2302) was purchased from American Type Culture Collection (Manassas, VA, USA) and used for experiments. Dulbecco's Modified Eagle's Medium/F12 (Sigma-Aldrich) containing 1% penicillin/streptomycin (Sigma-Aldrich) and 10% fetal bovine serum was used for culture medium. Medium was changed every 2 days. Cells in the range of passages 3–16 were used for studies. All experiments were performed after serum starvation.

### Preparation of ApoM-SIP

SIP was obtained from Enzo Life Sciences, inc. (Exeter, UK), and dissolved in methanol at 0.5 mg/mL. Before use in experiments, the methanol was evaporated using nitrogen gas. Human recombinant ApoM was obtained from R&D Systems (Minneapolis, MN, USA) and combined to create the ApoM-SIP complex as previously described<sup>42</sup>. SIP was dissolved in ApoM, followed by 45 minutes of incubation at room temperature.

### Preparation of FITC labeled POS

POS were labeled with FITC as previously described<sup>55</sup>. Briefly, POS were incubated with fluorescein-t-isothiocyanate (FITC 'Isomer I') from ThermoFisher Scientific (Waltham, MA, USA) for 1 hour and washed thoroughly with PBS.

### Treatment of ARPE-19 and ex vivo eyecups

To challenge RPE cells with photoreceptor outer segments, POS were obtained from InVision BioResources (Seattle, WA, USA). For ARPE-19, cells were allowed to adhere overnight in chamber slides from Ibidi (Germany). Media was exchanged for POS rich media at a 10:1 or 20:1 POS to RPE ratio as described previously<sup>55</sup>. Cells were incubated for 4 hours at 37 °C in a humidified cell culture incubator with 5% CO<sub>2</sub>. After incubation, ApoM-SIP that was previously prepared was added and incubated for 1 hour at 37 °C in a humidified cell culture incubation with 5% CO<sub>2</sub> after three washes with PBS. Cells were then washed thrice with PBS, fixed with 4% paraformaldehyde for 20 minutes at room temperature, and processed for analysis. For ex vivo eyecups, mice were first sacrificed and enucleated. Eyes were carefully dissected to remove the cornea, lens, and retina. The remaining eyecup was placed in a 96-well U-bottom plate from Corning (Corning, NY, USA) with either control DMEM/F12 or media enriched with POS-FITC. The plate was then incubated for 2 hours at 37 °C in a humidified cell culture incubator with 5% CO<sub>2</sub>. After incubation, ApoM-SIP that was previously prepared was added and incubated for 1 hour at 37 °C in a humidified cell culture incubation with 5% CO<sub>2</sub> after three washes with PBS. After three more PBS washes, eyecups were fixed for 20 minutes with 4% paraformaldehyde at room temperature. Eyecups were then immunohistologically stained and mounted onto a glass slide for imaging. To test for the effects of lipophagy inhibition, ARPE19 cells were seeded in 12-well chamber slides precoated with 1% Gelatin solution (Cell Biologicals, Cat. No. 6950) to aid adherence and maintained at 37 °C with 5% CO<sub>2</sub>. Cells were serum-starved overnight to remove exogenous sources of lipid. The next day, they were washed in DPBS and treated with bovine photoreceptor outer segments (POS) at 0, 10, or 20x ratio of POS:ARPE19 cells for 4 hr in serum-free media. Cells were washed in multiple changes of DPBS to remove POS followed by treatment with prepared ApoM-SIP (as described previously herein) and either DMSO (vehicle/control) or 30 μM Lalistat 2 (Axon Medchem, Cat. No. 2797) for 72 hr. Slides were washed in DPBS, fixed for 20 min at room temperature in prepared methanol-free 4% paraformaldehyde in PBS (Electron Microscopy Sciences, Cat. No. 15710) and stained with BODIPY, Alexfluor 594-conjugated phalloidin and DAPI as described herein. Images were acquired using an Olympus FV1000 confocal with a BX61-WI microscope and PlanApo N 60x TIRF Oil-immersion objective lens (1.45 N.A.) utilizing Fluoview software.

### Immunohistochemistry

After fixing either ARPE-19 or eyecups, cells were stained with 1:500 DAPI (ThermoFisher Scientific), 1:250 phalloidin-iFluor 594 (Abcam), and 1:250 BODIPY 493/503 (ThermoFisher Scientific) in PBS with 0.3% triton-X100 (Sigma-Aldrich) for 20 minutes at room temperature. Cells were then washed thrice with PBS before mounting and imaging. BODIPY fluorescence was quantified by ImageJ software through the RGB measure plugin.

### Cholesterol efflux assay

Cholesterol efflux of ARPE-19 cells with the addition of ApoM-SIP was assessed using the cholesterol efflux assay kit (ab196985) from Abcam (Cambridge, UK) according to the manufacturer's protocol. Briefly, ARPE-19 cells were allowed to adhere overnight in a 96-well tissue culture plate. Cells were loaded with fluorescently labeled cholesterol before being treated with a cholesterol acceptor. Serum from ApoM<sup>KO</sup> mice was prepared as a cholesterol acceptor, so cells treated with ApoM-SIP had the complex mixed in with serum from ApoM<sup>KO</sup> mice. Fluorescence intensity of the supernatant and cell lysates was assessed with a microplate reader to then calculate a percentage of cholesterol efflux.

### Reporting summary

Further information on research design is available in the Nature Portfolio Reporting Summary linked to this article.

### Data availability

All data from publicly available datasets analyzed are included in this published article (DOI: 10.1101/jcmm.16569) and the Gene Expression Omnibus (<https://www.ncbi.nlm.nih.gov/geo/>) through accession number GSE159435. Source data are provided with this paper. Any data supporting the findings from the study will be made readily available from the corresponding author upon request. Source data are provided with this paper.

### References

1. Apte, R. S. Age-related macular degeneration. *N. Engl. J. Med* **385**, 539–547 (2021).
2. Wong, W. L. et al. Global prevalence of age-related macular degeneration and disease burden projection for 2020 and 2040: a systematic review and meta-analysis. *Lancet Glob. Health* **2**, e106–e116 (2014).
3. Rein, D. B. et al. Prevalence of age-related macular degeneration in the US in 2019. *JAMA Ophthalmol.* **140**, 1202–1208 (2022).
4. Sene, A. et al. Impaired cholesterol efflux in senescent macrophages promotes age-related macular degeneration. *Cell Metab.* **17**, 549–561 (2013).
5. Curcio, C. A. Antecedents of Soft Drusen, the specific deposits of age-related macular degeneration, in the biology of human Macula. *Invest Ophthalmol. Vis. Sci.* **59**, AMD182–AMD194 (2018).
6. Ferris, F. L. III, Fine, S. L. & Hyman, L. Age-related macular degeneration and blindness due to neovascular maculopathy. *Arch. Ophthalmol.* **102**, 1640–1642 (1984).
7. Apte, R. S. Targeting tissue lipids in age-related macular degeneration. *EBioMedicine* **5**, 26–27 (2016).
8. Apte, R. S., Chen, D. S. & Ferrara, N. VEGF in signaling and disease: beyond discovery and development. *Cell* **176**, 1248–1264 (2019).
9. The Age-Related Eye Disease Study 2 (AREDS2) Research Group\* Lutein + Zeaxanthin and Omega-3 fatty acids for age-related macular degeneration: The Age-Related Eye Disease Study 2 (AREDS2) randomized clinical trial. *JAMA* **309**, 2005–2015 (2013).
10. Yang, S., Zhao, J. & Sun, X. Resistance to anti-VEGF therapy in neovascular age-related macular degeneration: a comprehensive review. *Drug Des. Dev. Ther.* **10**, 1857–1867 (2016).
11. Vishwakarma, S. & Kaur, I. Molecular mediators and regulators of retinal angiogenesis. *Semin. Ophthalmol.* **38**, 124–133 (2023).
12. Khachigian, L. M., Liew, G., Teo, K. Y. C., Wong, T. Y. & Mitchell, P. Emerging therapeutic strategies for unmet need in neovascular age-related macular degeneration. *J. Transl. Med.* **21**, 133 (2023).
13. Liao, D. S. et al. Complement C3 inhibitor Pegcetacoplan for geographic atrophy secondary to age-related macular degeneration: a randomized Phase 2 trial. *Ophthalmology* **127**, 186–195 (2020).

14. Wilke, G. A. & Apte, R. S. Complement regulation in the eye: implications for age-related macular degeneration. *J. Clin. Invest.* **134**, e178296.
15. Cheung, C. M. G. et al. Plasma lipoprotein subfraction concentrations are associated with lipid metabolism and age-related macular degeneration. *J. Lipid Res.* **58**, 1785–1796 (2017).
16. Danis, R. P., Lavine, J. A. & Domalpally, A. Geographic atrophy in patients with advanced dry age-related macular degeneration: current challenges and future prospects. *Clin. Ophthalmol.* **9**, 2159–2174 (2015).
17. Handa, J. T. et al. A systems biology approach towards understanding and treating non-neovascular age-related macular degeneration. *Nat. Commun.* **10**, 3347 (2019).
18. Malek, G., Li, C.-M., Guidry, C., Medeiros, N. E. & Curcio, C. A. Apolipoprotein B in cholesterol-containing drusen and basal deposits of human eyes with age-related maculopathy. *Am. J. Pathol.* **162**, 413–425 (2003).
19. Martin, S. S. et al. Comparison of high-density lipoprotein cholesterol to Apolipoprotein A-I and A-II to predict coronary calcium and the effect of insulin resistance. *Am. J. Cardiol.* **107**, 393–398 (2011).
20. Shen, L. L. et al. Associations of systemic health and medication use with the enlargement rate of geographic atrophy in age-related macular degeneration. *Br. J. Ophthalmol.* **107**, 261–266 (2023).
21. Winkler, T. W. et al. Genome-wide association meta-analysis for early age-related macular degeneration highlights novel loci and insights for advanced disease. *BMC Med Genom.* **13**, 120 (2020).
22. Strunz, T., Kiel, C., Sauerbeck, B. L. & Weber, B. H. F. Learning from fifteen years of genome-wide association studies in age-related macular degeneration. *Cells* **9**, 2267 (2020).
23. Landowski, M. & Bowes Rickman, C. Targeting lipid metabolism for the treatment of age-related macular degeneration: insights from preclinical mouse models. *J. Ocul. Pharm. Ther.* **38**, 3–32 (2022).
24. Kelly, U. L. et al. High-density lipoproteins are a potential therapeutic target for age-related macular degeneration. *J. Biol. Chem.* **295**, 13601–13616 (2020).
25. Rudolf, M. et al. Sub-retinal drusenoid deposits in human retina: Organization and composition. *Exp. Eye Res.* **87**, 402–408 (2008).
26. Ban, N. et al. Disrupted cholesterol metabolism promotes age-related photoreceptor neurodegeneration. *J. Lipid Res.* [jlr.M084442](https://doi.org/10.1194/jlr.M084442) <https://doi.org/10.1194/jlr.M084442>. (2018).
27. Storti, F. et al. Impaired ABCA1/ABCG1-mediated lipid efflux in the mouse retinal pigment epithelium (RPE) leads to retinal degeneration. *eLife* **8**, e45100.
28. Ban, N. et al. Impaired monocyte cholesterol clearance initiates age-related retinal degeneration and vision loss. *JCI Insight* **3**, e120824 (2018).
29. Terao, R. et al. LXR/CD38 activation drives cholesterol-induced macrophage senescence and neurodegeneration via NAD<sup>+</sup> depletion. *Cell Rep.* 114102 <https://doi.org/10.1016/j.celrep.2024.114102>. (2024).
30. Wolfrum, C., Poy, M. N. & Stoffel, M. Apolipoprotein M is required for pre $\beta$ -HDL formation and cholesterol efflux to HDL and protects against atherosclerosis. *Nat. Med* **11**, 418–422 (2005).
31. Ding, B.-S. et al. Aging Suppresses Sphingosine-1-Phosphate Chaperone ApoM in circulation resulting in maladaptive organ repair. *Dev. Cell* **53**, 677–690.e4 (2020).
32. Christoffersen, C. et al. Endothelium-protective sphingosine-1-phosphate provided by HDL-associated apolipoprotein M. *Proc. Natl. Acad. Sci. USA* **108**, 9613–9618 (2011).
33. Christoffersen, C. et al. Isolation and characterization of human apolipoprotein M-containing lipoproteins. *J. Lipid Res.* **47**, 1833–1843 (2006).
34. Xu, N. & Dahlbäck, B. A Novel Human Apolipoprotein (apoM)\*. *J. Biol. Chem.* **274**, 31286–31290 (1999).
35. Liu, M. et al. Hepatic Apolipoprotein M (ApoM) overexpression stimulates formation of larger ApoM/Sphingosine 1-Phosphate-enriched plasma high density Lipoprotein. *J. Biol. Chem.* **289**, 2801–2814 (2014).
36. Elsåe, S. et al. Apolipoprotein M binds oxidized phospholipids and increases the antioxidant effect of HDL. *Atherosclerosis* **221**, 91–97 (2012).
37. Christoffersen, C. et al. Effect of Apolipoprotein M on high density lipoprotein metabolism and atherosclerosis in low density lipoprotein receptor knock-out mice\*. *J. Biol. Chem.* **283**, 1839–1847 (2008).
38. Christensen, P. M. et al. Impaired endothelial barrier function in apolipoprotein M-deficient mice is dependent on sphingosine-1-phosphate receptor 1. *FASEB J.* **30**, 2351–2359 (2016).
39. Ruiz, M., Okada, H. & Dahlbäck, B. HDL-associated ApoM is anti-apoptotic by delivering sphingosine 1-phosphate to S1P1 & S1P3 receptors on vascular endothelium. *Lipids Health Dis.* **16**, 36 (2017).
40. Guo, Z. et al. Apolipoprotein M attenuates anthracycline cardiotoxicity and lysosomal injury. *JACC Basic Transl. Sci.* **8**, 340–355 (2023).
41. Terao, R. et al. The role of sphingosine 1-phosphate receptors on retinal pigment epithelial cells barrier function and angiogenic effects. *Prostaglandins Other Lipid Mediat.* **145**, 106365 (2019).
42. Terao, R., Honjo, M. & Aihara, M. Apolipoprotein M inhibits angiogenic and inflammatory response by Sphingosine 1-Phosphate on retinal pigment epithelium cells. *Int J. Mol. Sci.* **19**, 112 (2017).
43. Vaidya, M. et al. Regulation of ABCA1-mediated cholesterol efflux by sphingosine-1-phosphate signaling in macrophages. *J. Lipid Res.* **60**, 506–515 (2019).
44. Raposo, G. & Marks, M. S. The dark side of lysosome-related organelles: specialization of the endocytic pathway for melanosome biogenesis. *Traffic* **3**, 237–248 (2002).
45. Schraermeyer, U., Peters, S., Thumann, G., Kociok, N. & Heimann, K. Melanin granules of retinal pigment epithelium are connected with the lysosomal degradation pathway. *Exp. Eye Res.* **68**, 237–245 (1999).
46. Kim, I. T. & Choi, J. B. Melanosomes of retinal pigment epithelium-distribution, shape, and acid phosphatase activity. *Korean J. Ophthalmol.* **12**, 85–91 (1998).
47. Chirinos, J. A. et al. Reduced Apolipoprotein M and adverse outcomes across the spectrum of human heart failure. *Circulation* **141**, 1463–1476 (2020).
48. Bosteen, M. H., Dahlbäck, B., Nielsen, L. B. & Christoffersen, C. Protein unfolding allows use of commercial antibodies in an apolipoprotein M sandwich ELISA. *J. Lipid Res* **56**, 754–759 (2015).
49. Tsin, A., Betts-Obregon, B. & Grigsby, J. Visual cycle proteins: Structure, function, and roles in human retinal disease. *J. Biol. Chem.* **293**, 13016–13021 (2018).
50. Lee, T. J. et al. Catalytic isoforms of AMP-activated protein kinase differentially regulate IMPDH activity and photoreceptor neuron function. *JCI Insight* <https://doi.org/10.1172/jci.insight.173707>. (2024).
51. Butler, J. M., Supharattanasitthi, W., Yang, Y. C. & Paraoan, L. RNA-seq analysis of ageing human retinal pigment epithelium: Unexpected up-regulation of visual cycle gene transcription. *J. Cell Mol. Med.* **25**, 5572–5585 (2021).
52. Goldberg, A. F. X., Moritz, O. L. & Williams, D. S. Molecular basis for photoreceptor outer segment architecture. *Prog. Retin. Eye Res.* **55**, 52–81 (2016).
53. Albert, A., Alexander, D. & Boesze-Battaglia, K. Cholesterol in the rod outer segment: A complex role in a “simple” system. *Chem. Phys. Lipids* **199**, 94–105 (2016).
54. Storti, F. et al. Regulated efflux of photoreceptor outer segment-derived cholesterol by human RPE cells. *Exp. Eye Res.* **165**, 65–77 (2017).

55. Mazzoni, F., Mao, Y. & Finnemann, S. C. Advanced analysis of photoreceptor outer segment phagocytosis by RPE cells in culture. *Methods Mol. Biol.* **1834**, 95–108 (2019).
56. Yako, T., Otsu, W., Nakamura, S., Shimazawa, M. & Hara, H. Lipid droplet accumulation promotes RPE dysfunction. *Int J. Mol. Sci.* **23**, 1790 (2022).
57. Rosario, F.-G., Garland, D. L. & Pierce, E. A. Isolation, culture and characterization of primary mouse RPE cells. *Nat. Protoc.* **11**, 1206–1218 (2016).
58. Zhang, S. et al. The regulation, function, and role of lipophagy, a form of selective autophagy, in metabolic disorders. *Cell Death Dis.* **13**, 132 (2022).
59. Du, H., Duanmu, M., Witte, D. & Grabowski, G. A. Targeted disruption of the mouse lysosomal acid lipase gene: long-term survival with massive cholesteryl ester and triglyceride storage. *Hum. Mol. Genet.* **7**, 1347–1354 (1998).
60. Leopold, C. et al. Hepatocyte-specific lysosomal acid lipase deficiency protects mice from diet-induced obesity but promotes hepatic inflammation. *Biochim. et. Biophys. Acta (BBA) - Mol. Cell Biol. Lipids* **1864**, 500–511 (2019).
61. Nolan, N. D., Jenny, L. A., Wang, N.-K. & Tsang, S. H. Retinal pigment epithelium lipid metabolic demands and therapeutic restoration. *Taiwan J. Ophthalmol.* **11**, 216–220 (2021).
62. Kono, M. et al. The Sphingosine-1-phosphate Receptors S1P1, S1P2, and S1P3 Function Coordinately during Embryonic Angiogenesis \*. *J. Biol. Chem.* **279**, 29367–29373 (2004).
63. Allende, M. L., Yamashita, T. & Proia, R. L. G-protein-coupled receptor S1P1 acts within endothelial cells to regulate vascular maturation. *Blood* **102**, 3665–3667 (2003).
64. Du, H. et al. Lysosomal acid lipase-deficient mice: depletion of white and brown fat, severe hepatosplenomegaly, and shortened life span. *J. Lipid Res.* **42**, 489–500 (2001).
65. Xue, Y., Shen, S. Q., Corbo, J. C. & Kefalov, V. J. Circadian and light-driven regulation of rod dark adaptation. *Sci. Rep.* **5**, (2015).
66. Lee, T. J. Mechanisms of rod photoreceptor metabolism and function in health and disease. *Arts Sci. Electron. Theses Dissert.* 3037. [https://openscholarship.wustl.edu/art\\_sci\\_etds/3037](https://openscholarship.wustl.edu/art_sci_etds/3037). (2024).

## Acknowledgements

This work was supported by National Institutes of Health (NIH) grants R01 EY019287 (RSA) and P30 EY02687 (Vision Core Grant); Jeffrey T. Fort Innovation Fund (RSA); Starr Foundation AMD Research Fund (RSA); Siteman Retina Research Fund (RSA); Carl Marshall and Mildred Almen Reeves Foundation (RSA); Retina Associates of St. Louis Research Fund (RSA); a pilot project grant from the Washington University Genome Technology Access Center (RSA); Research to Prevent Blindness/American Macular Degeneration Foundation Catalyst Award for Innovative Research Approaches for Age-Related Macular Degeneration (RSA) and an unrestricted grant from Research to Prevent Blindness to the John F. Hardesty, MD Department of Ophthalmology and Visual Sciences at Washington University School of Medicine in St. Louis. The authors thank the families of the generous tissue donors, the Mid-America Transplant Eye Bank for their collection of human tissue used in this study, and the Bright Center for Human Vision at WashU Medicine for the distribution of human tissue samples for research. TL was supported by NIH Training Grant (1T32GM1397740-1) and Vitreoretinal Surgery Foundation Fellowship (VGR0023118). AJ was supported by K08HL138262 and 1R01HL155344 from the NHLBI and by the Children's Discovery Institute of Washington University and St. Louis Children's Hospital (MC-FR-2020- 919), as well as the Diabetes Research Center at

Washington University in St. Louis of the National Institutes of Health under award number P30DK020579, and the NIH grant P30DK056341 (Nutrition Obesity Research Center) and received support from the Longer Life Foundation. DK was supported by funding from the Austrian Science Fund (FWF) (SFB 10.55776/F73). The authors acknowledge Wandy L. Beatty, Molecular Microbiology Imaging Facility in Washington University School of Medicine, for electron microscopy analyses. This manuscript re-used the data and results from the thesis and dissertation of the first author, T.J.L., that have been previously published<sup>66</sup>.

## Author contributions

T.J.L., R.S.A. and A.J. designed and analyzed the experiments. T.J.L., A.S., K.P., C.V.P., R.T., Z.G., M.O. and C.C. conducted the experiments. D.K., C.C., A.J., and R.S.A. provided resources. T.J.L., R.S.A. and A.J. designed the methodology and wrote the manuscript. T.J.L., R.S.A. and A.J. conceptualized the study.

## Competing interests

RSA and AJ have intellectual property applications licensed by Washington University to Mobius Scientific. RSA and AJ are on the advisory board of Mobius Scientific, and RSA is currently the CSO at Mobius Scientific. The remaining authors declare no competing interests.

## Additional information

**Supplementary information** The online version contains supplementary material available at <https://doi.org/10.1038/s41467-025-60830-1>.

**Correspondence** and requests for materials should be addressed to Ali Javaheri or Rajendra S. Apte.

**Peer review information** *Nature Communications* thanks Makoto Kurano, Yoko Ozawa, and the other anonymous reviewer(s) for their contribution to the peer review of this work. A peer review file is available.

**Reprints and permissions information** is available at <http://www.nature.com/reprints>

**Publisher's note** Springer Nature remains neutral with regard to jurisdictional claims in published maps and institutional affiliations.

**Open Access** This article is licensed under a Creative Commons Attribution-NonCommercial-NoDerivatives 4.0 International License, which permits any non-commercial use, sharing, distribution and reproduction in any medium or format, as long as you give appropriate credit to the original author(s) and the source, provide a link to the Creative Commons licence, and indicate if you modified the licensed material. You do not have permission under this licence to share adapted material derived from this article or parts of it. The images or other third party material in this article are included in the article's Creative Commons licence, unless indicated otherwise in a credit line to the material. If material is not included in the article's Creative Commons licence and your intended use is not permitted by statutory regulation or exceeds the permitted use, you will need to obtain permission directly from the copyright holder. To view a copy of this licence, visit <http://creativecommons.org/licenses/by-nc-nd/4.0/>.

© The Author(s) 2025